ResearchGate

See discussions, stats, and author profiles for this publication at: https://www.researchgate.net/publication/261765959

Rate Constants and Kinetic Isotope Effects for Methoxy Radical Reacting with NO2 and O-2

ARTICLE *in* THE JOURNAL OF PHYSICAL CHEMISTRY A · APRIL 2014

Impact Factor: 2.69 · DOI: 10.1021/jp501205d · Source: PubMed

CITATIONS
3

READS
28

5 AUTHORS, INCLUDING:

Jiajue Chai
Brown University
8 PUBLICATIONS **16** CITATIONS
SEE PROFILE

Hongyi Hu
Syracuse University
7 PUBLICATIONS **38** CITATIONS
SEE PROFILE

Theodore S Dibble
State University of New York College of Enviro…
79 PUBLICATIONS **1,026** CITATIONS
SEE PROFILE

Available from: Theodore S Dibble
Retrieved on: 26 January 2016

THE JOURNAL OF PHYSICAL CHEMISTRY A

Article

pubs.acs.org/JPCA

Rate Constants and Kinetic Isotope Effects for Methoxy Radical Reacting with NO_2 and O_2

Jiajue Chai, Hongyi Hu, and Theodore S. Dibble*

Department of Chemistry, College of Environmental Science and Forestry, State University of New York, Syracuse, New York 13210, United States

Geoffrey S. Tyndall* and John J. Orlando

Atmospheric Chemistry Division, National Center for Atmospheric Research, Boulder, Colorado 80307, United States

Supporting Information

ABSTRACT: Relative rate studies were carried out to determine the temperature dependent rate constant ratio k_1/k_{2a}: $CH_3O\cdot + O_2 \rightarrow HCHO + HO_2\cdot$ and $CH_3O\cdot + NO_2$ (+M) $\rightarrow CH_3ONO_2$ (+M) over the temperature range 250−333 K in an environmental chamber at 700 Torr using Fourier transform infrared detection. Absolute rate constants k_2 were determined using laser flash photolysis/laser-induced fluorescence under the same conditions. The analogous experiments were carried out for the reactions of the perdeuterated methoxy radical ($CD_3O\cdot$). Absolute rate constants k_2 were in excellent agreement with the recommendations of the JPL Data Evaluation panel. The combined data (i.e., k_1/k_2 and k_2) allow the determination of k_1 as $1.3^{+0.9}_{-0.5} \times 10^{-14}$ exp[−(663 ± 144)/T] cm^3 s^{-1}, corresponding to 1.4×10^{-15} cm^3 s^{-1} at 298 K. The rate constant at 298 K is in excellent agreement with previous work, but the observed temperature dependence is less than was previously reported. The deuterium isotope effect, k_H/k_D, can be expressed in the Arrhenius form as $k_1/k_3 = (1.7^{+0.5}_{-0.4})$ exp((306 ± 70)/T). The deuterium isotope effect does not appear to be greatly influenced by tunneling, which is consistent with a previous theoretical work by Hu and Dibble. (Hu, H.; Dibble, T. S., *J. Phys. Chem. A* **2013**, *117*, 14230−14242.)

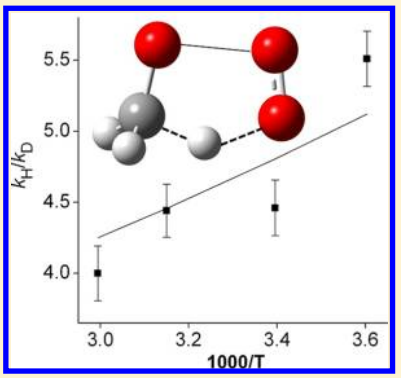

I. INTRODUCTION

Alkoxy radicals (RO·) are important intermediates in the photooxidation of volatile organic compounds (VOCs) in the troposphere. The fates of alkoxy radicals (unimolecular decomposition and isomerization, and reactions with O_2) greatly impact ozone formation in the troposphere as well as gas-particle partitioning of the eventual stable products.[1,2] To date, direct kinetic studies of RO· + O_2 have been limited to alkoxy radicals derived from C_1—C_7 alkanes[3−15] and two halogenated alkanes.[16−18] Many previous studies of alkoxy radical kinetics have only determined the rate constant ratio for the unimolecular decomposition and the reaction with O_2 ($k_{unimolecular}/k_{O2}$) and have relied upon an estimate of k_{O2} to determine $k_{unimolecular}$. The lack of absolute rate constants, k_{O2}, obstructs the determination of $k_{unimolecular}$, thus preventing us from establishing accurate structure−activity relations (SARs) for the unimolecular reactions. SARs are needed to enable the prediction of the tropospheric fate of larger and functionalized alkoxy radicals, for which experimental data is largely absent and difficult to obtain from experiments.[19,20]

The methoxy radical ($CH_3O\cdot$) is the prototype for all alkoxy radicals. Similarly, the kinetics and mechanism of the methoxy + O_2 reaction R1

$$CH_3O\cdot + O_2 \xrightarrow{k_1} HCHO + HO_2\cdot \qquad (R1)$$

is the prototype for other RO· + O_2 reactions. Both absolute and relative rate studies were carried out to determine k_1. Rate constant ratios for R1 versus $CH_3O\cdot$ + NO or NO_2 were reported for $296 \le T \le 450$ K by various groups in the 1970s.[21−26] These efforts used product analysis following the photolysis of methylnitrite (CH_3ONO) or the pyrolysis of dimethyl peroxide (CH_3OOCH_3) or CH_3ONO. The rate constant ratios obtained in these experiments exhibit a lot of scatter, and only the result of Cox et al.[23] at room temperature agrees well with absolute rate studies. Three absolute measurements of k_1 over $298 \le T \le 973$ K were conducted using laser flash photolysis-laser induced fluorescence (LFP-LIF), with either CH_3ONO or CH_3OH used as the $CH_3O\cdot$ precursor.[3−5] These results are in general agreement in their range of overlap ($298 \le T \le 610$ K), and were fitted by an Arrhenius expression: $k_1 = 7.82^{+4.68}_{-2.93} \times 10^{-14}$ exp[−(1150 ± 190)/T] cm^3 s^{-1}, with quoted uncertainties of two standard deviations.[19] At 298 K, this expression yields $k_1 = 1.6 \times 10^{-15}$ cm^3 s^{-1}. Rate constants obtained at $T > 610$ K greatly exceed those obtained by an extrapolation of an Arrhenius plot of the data at lower temperatures.[3] Notably, no measurement of k_1 has

Received: February 3, 2014
Revised: April 17, 2014
Published: April 18, 2014

ACS Publications © 2014 American Chemical Society

been done below room temperature. This is because k_1 is small and becomes smaller as temperature decreases, so that the use of a high concentration of O_2 (>50 Torr) is required. Unfortunately, O_2 efficiently quenches fluorescence of excited $CH_3O\cdot$ ($\tilde{A}^2A_1$).[27]

To overcome the difficulty of directly measuring k_1 below room temperature, we combined measurements of the ratio k_1/k_2 with the absolute determination of k_2, where k_2 is the overall rate constant for the reaction of $CH_3O\cdot$ with NO_2:

$$CH_3O\cdot + NO_2(+M) \xrightarrow{k_{2a}} CH_3ONO_2(+M) \quad \text{(R2a)}$$

$$CH_3O\cdot + NO_2 \xrightarrow{k_{2b}} HCHO + HNO_2 \quad \text{(minor)} \quad \text{(R2b)}$$

Measurements were carried out over the temperature range 250−335 K. The rate constant ratio (k_1/k_2) was measured at the National Center for Atmospheric Research (NCAR) in a smog chamber based on product analysis by Fourier transform infrared (FTIR) spectroscopy. The absolute rate constants k_2 were measured at State University of New York's College of Environmental Science and Forestry (SUNY-ESF) using LFP-LIF. By combining the two measurements, the absolute rate constant k_1 was determined as a function of temperature.

The kinetics of methoxy + NO_2 (R2) are important to interpret smog chamber experiments, where NO_x concentrations are often much higher than in the atmosphere. It is widely agreed that the reaction between $CH_3O\cdot$ and NO_2 can proceed via two channels—recombination (R2a) producing methylnitrate (CH_3ONO_2), and disproportionation (R2b) yielding formaldehyde and nitrous acid. McCaulley et al. reported a rate constant of $9.6^{+17.3}_{-2.7} \times 10^{-12} \exp(-(1150^{+550}_{-170})/T)$ cm^3 s^{-1} for the disproportionation channel, which is only significant at rather low pressures, for example, $k_{2b}/k_{2a} \approx 0.1$ at 1 Torr and 298 K.[28,29] At higher pressures, the recombination channel becomes even more dominant.[28−33] Direct kinetic investigations of R2 (using LIF detection of $CH_3O\cdot$) were carried out at pressures up to 600 Torr over the temperature range 220−473 K with Ar, CF_4, or He as bath gases. All of these studies showed a broadly similar pressure-dependent behavior of k_2; however, the values from the two studies with the largest pressure ranges differ by 30%. Because of the inconsistencies of previous reports of k_2, it is valuable to re-examine this rate constant and especially to use a buffer gas more representative of air than Ar, CF_4, or He.

We also investigated the deuterium kinetic isotope effect (KIE) of the methoxy + O_2 reaction by substituting $CD_3O\cdot$ for $CH_3O\cdot$:

$$CD_3O\cdot + O_2 \rightarrow DCDO + DO_2 \quad \text{(R3)}$$

$$CD_3O\cdot + NO_2(+M) \rightarrow CD_3ONO_2 \quad \text{(R4a)}$$

$$CD_3O\cdot + NO_2 \rightarrow DCDO + DNO_2 \quad \text{(minor)} \quad \text{(R4b)}$$

over the temperature range of 250−333 K, using the same method of combining the measurement of the ratio k_3/k_4 with the absolute measurement of k_4. KIE is defined as k_H/k_D—the rate constant ratio between the reaction involving the nondeuterated reactant and that involving the deuterated reactant; here KIEs for methoxy + O_2 and methoxy + NO_2 are k_1/k_3 and k_2/k_4, respectively.

No kinetic studies have been reported for either R3 or R4, except for one relative rate study that estimated k_3 as $(8.0-21) \times 10^{-18}$ cm^3 s^{-1} at 298 K.[34] This value would imply a KIE of about 100 at 298 K. Even if this KIE estimate is high, the value of k_3 is expected to be significantly smaller than k_1, thus making measurement of k_3 by the LFP-LIF method extremely difficult even at room temperature.

A long-term goal of ours is to better understand the kinetics of alkoxy + O_2 reactions, including the role of tunneling. Several theoretical studies have tried to elucidate the mechanism of $CH_3O\cdot$ + O_2. Jungkamp and Seinfeld proposed that the reaction occurs via the formation of a short-lived trioxy radical intermediate followed by HO_2 elimination.[35] This mechanism is consistent with the unusually low Arrhenius pre-exponential factor (*A*-factor) for the reaction; however, Bofill et al.[36] found an error in the work on this mechanism and reported an enormous barrier (50 kcal/mol) to HO_2 elimination from the trioxy radical intermediate. Instead, Bofill et al. found that H-abstraction, while direct, occurs through a five-member ring-like transition state structure that accounts for the low *A*-factor.[36] On the basis of this mechanism, both Bofill et al.[36] and Setokuchi and Sato[37] calculated k_1 in good agreement with this experiment. Curiously, these two groups found very different tunneling corrections (κ) to the rate constant at 298 K. Bofill et al. found $\kappa = 9$ using the asymmetric Eckart model, while Setokuchi and Sato found κ of about 2 using a multidimensional tunneling approach. Recently Hu and Dibble carried out calculations on three isotopologues of the methoxy + O_2 reaction.[38] These calculations further confirmed the reaction mechanism of Bofill et al.,[36] and obtained tunneling corrections similar to those of Setokuchi and Sato.[37] These calculations also agreed remarkably well with our previously reported experimental branching ratio for hydrogen- versus deuterium-abstraction in the reaction $CH_2DO\cdot$ + O_2.[39]

In the following section, we present the experimental method for investigating the rate constant ratios R1/R2a and R3/R4a in the chamber at the NCAR. This is followed by a description of the absolute rate constant measurement of R2 and R4 at SUNY-ESF. We then present analyses of the relative rate measurements and kinetic modeling efforts used to understand the effects of secondary chemistry on the observed product concentrations in the chamber experiments. Next we present the absolute rate constant measurements of R2 and R4 and combine the absolute and relative rate data to yield rate constants for R1 and R3. This is followed by a comparison with previous rate constant determinations and a discussion of KIEs.

II. EXPERIMENTAL SECTION

II-1. Preparation of Gaseous Reactants. The photolytic precursor of the methoxy radical, methylnitrite (CH_3ONO or CD_3ONO) was synthesized from the corresponding methyl alcohol (CH_3OH, Sigma-Aldrich, 99.8%; CD_3OH, Sigma-Aldrich, 99.8%).[40,41] The reaction was initiated by the dropwise addition of concentrated (58% by mass) sulfuric acid solution into an aqueous solution of $NaNO_2$ and methanol at 0 °C. The resulting gaseous products were transferred by N_2 gas over a NaOH solution and then over anhydrous $CaCl_2$, and were finally collected in a dry ice trap at −78 °C. The isolated product was purified by freeze−pump−thaw distillation, resulting in a pale yellow, glassy solid, which was stored at −196 °C until it was used. Gaseous methylnitrite was characterized by FTIR[42] and UV−vis spectroscopy, and the absence of residual methanol was verified.[41,43] NO_2 was produced by mixing NO (American Gas Group, >99.5%) with a large excess of O_2 (MG Welding Products or U.S.

dx.doi.org/10.1021/jp501205d | J. Phys. Chem. A 2014, 118, 3552−3563

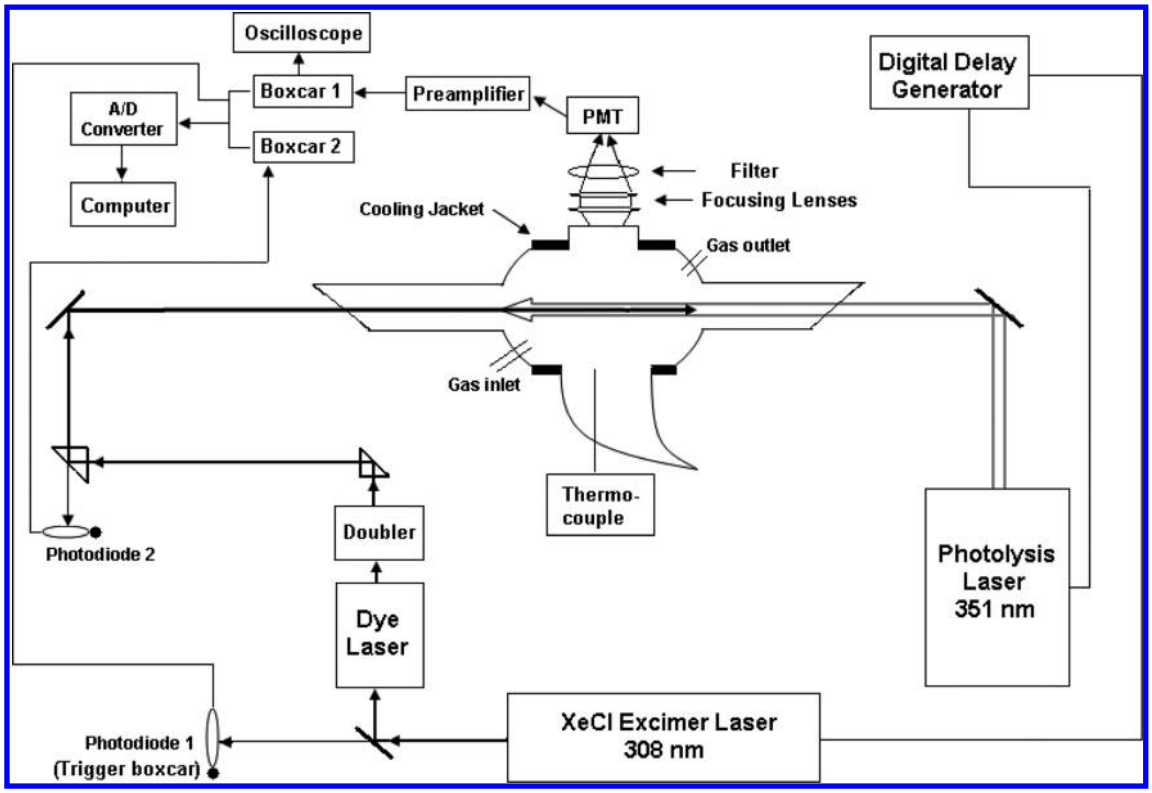

Figure 1. The LFP-LIF apparatus described in the text.

Welding, 99.999%), and was purified by freeze−pump−thaw distillation at −196 °C until a pure white solid was obtained. The resultant NO_2 was checked for purity via FTIR[44] and UV−vis spectroscopy.[45]

In both experiments, the purified methylnitrite was first transferred into a blackened glass bulb, which was then diluted by bath gas N_2 (in the LFP-LIF experiment, Haun Welding Supply, 99.999%; in the chamber experiment, General Air, liquid nitrogen boil-off) to a total pressure of 1000 Torr. This resulted in ∼3% methylnitrite in N_2. NO_2 was diluted with N_2 in another blackened glass bulb, with a molar percentage of ∼2%. Concentrations of methylnitrite and NO_2 in the gas bulbs were determined using UV−vis absorption cross sections[41,45] of multiple peaks in the range of 310−370 nm and 380−440 nm, respectively. Concentrations were determined with a precision (1 σ) of 3%.

II-2. Experimental Methods and Materials. *II-2-1. Relative Rate Measurement.* Relative rate measurements were performed at the NCAR using a 2 m long, 47 L cylindrical stainless steel chamber. The details of the apparatus were reported elsewhere.[46,47] The concentrations of the chemicals of interest in the chamber were measured using a FTIR spectrometer (BOMEM DA3.01). The chamber consists of three concentric cylinders: the outer cylinder is evacuated for insulation, the middle cylinder has heating/cooling fluid circulated through it, and the inner cylinder contains gases and optics. Multipass Hanst-type optical mirrors sit at both ends of the chamber, enabling the path length of the IR light beam to reach 32.6 m. The resolution of the spectra in the experiment was 1 cm^{-1}, which is a good compromise between the sensitivity and speed of analysis. Thermocouples located around the chamber measure the temperature, which was controlled to within 0.1 K. The filtered output of a Xe-arc lamp located at one end of the chamber provided light between 285 and 400 nm to initiate the reaction by photolysis.

The initial reactants in the chamber for each set of experiments are methylnitrite (CH_3ONO or CD_3ONO), O_2, and NO_2. Photolysis of methylnitrite generates methoxy radicals that react with O_2 and NO_2 competitively via R1 and R2 (or R3 and R4). Reference spectra of the reactants (methylnitrite, NO_2) and the products (formaldehyde (HCHO/DCDO), methylnitrate (CH_3ONO_2/CD_3ONO_2), and CO) were obtained at each temperature. The integrated IR cross-section of methylnitrite is estimated to be accurate to 5% (1 σ).

The procedure for obtaining the reference spectra of CH_3ONO_2/CD_3ONO_2 was as follows: Methylnitrite and NO_2 were flushed into the chamber with N_2, and extra N_2 was added until the chamber pressure reached 700 Torr. Infrared spectra were recorded before and after 40−60 min of photolysis. The resulting spectra included CH_3ONO/CD_3ONO, NO_2, CH_3ONO_2/CD_3ONO_2, and a small amount of formaldehyde. The reference spectrum of methylnitrate was obtained by subtracting the spectra of other species. The peak area (integrated intensity) at 1240−1340 cm^{-1} (symmetric N═O stretch) from a known concentration of standard isopropyl nitrate at 295 K was used to calibrate the reference spectra of CH_3ONO_2/CD_3ONO_2. Reference spectra were not obtained at temperatures below 277 K due to experimental difficulties. The reference spectra from 295 K was used to fit the nitrate spectra at 250 and 265 K, but the fitted concentration was insensitive to use of the 333 K reference spectra in place of the 295 K reference spectra. Measured band strengths of different alkylnitrates vary by about 10%,[48,49] so the use of readily available isopropyl nitrate to quantify methylnitrate concentrations should have introduced only modest error.

dx.doi.org/10.1021/jp501205d | J. Phys. Chem. A 2014, 118, 3552−3563

Reference spectra of HCHO/DCDO were obtained from gaseous HCHO and DCDO that were generated by heating normal and fully deuterated paraformaldehyde (Fluka), respectively. The concentrations of the HCHO reference spectra at temperatures other than 295 K were computed through the band strengths (1.36×10^{-17} cm molecule^{-1} at 1660−1820 cm^{-1}) of the calibrated HCHO reference spectra that were obtained at 295 K in this laboratory previously,[50] while the concentrations of DCDO were determined based on the reported band strengths at 1620−1770 cm^{-1} (9.70×10^{-18} cm molecule^{-1}).[51] Reference spectra of NO_2 were obtained at each temperature and were calibrated according to the reference spectra of NO_2 that was previously obtained at the NCAR at 295 K.[52] CO concentrations were determined on the basis of reference spectra obtained at the NCAR, as 1×10^{15} molecules cm^{-3} per unit peak absorbance (base e). The integrated IR cross-sections of formaldehyde and NO_2 are believed to be accurate to 3−5% (1 σ), and the peak height for CO is also estimated to be accurate to 5%.

Relative rate measurements for the $CH_3O\cdot$ and $CD_3O\cdot$ reactions were conducted in the temperature ranges of 250−333 K and 277−335 K, respectively. Concentrations of methylnitrite and the reaction products were determined by the spectral subtraction of calibrated reference spectra obtained in the laboratory. Each experiment started with about 3.7×10^{14} molecules cm^{-3} of methylnitrite in the chamber. The initial concentration ratio of O_2 to NO_2 ranged from approximately 2×10^3 to 7×10^4. The reactants in the chamber were buffered by N_2 gas to a total pressure of 700 ± 5 Torr.

For each set of measurements with a fixed initial concentration ratio of O_2 to NO_2, IR spectra were recorded before the photolysis started and at 10 min intervals after photolysis began until 60 min had elapsed. Concentrations of methylnitrite, formaldehyde, CO, and methylnitrate were obtained. Ideally, the ratio of the pseudo-first-order rate constants ($k'(O_2)/k'(NO_2)$) is proportional to the ratio between the formaldehyde concentration and the methylnitrate concentration. A preliminary value of the ratio $k'(O_2)/k'(NO_2)$ was obtained from the slope of the plot of the formaldehyde concentration versus the methylnitrate concentration, via the expression

$$\frac{k'(O_2)}{k'(NO_2)} = \frac{k(O_2) \times [O_2]}{k(NO_2) \times [NO_2]} = \frac{[CH_2O]}{[CH_3ONO_2]} \quad (1)$$

At each temperature, at least five sets of experiments were done with various ratios of $[O_2]$ and $[NO_2]$.

II-2-2. Absolute Rate Constant—LFP-LIF Method. The LIF apparatus is shown in Figure 1 and is a modified version of one used at SUNY-ESF previously.[14,53] A pulsed XeF excimer laser (GAM Laser Inc., EX100H) with energy of 10 mJ/pulse and a repetition rate of 2 Hz was used to generate $CH_3O\cdot$ or $CD_3O\cdot$ by photolyzing CH_3ONO or CD_3ONO at 351 nm. The resulting methoxy radicals were probed via the ($\tilde{A}\ ^2A_1 \leftarrow \tilde{X}^2E$) system at ∼293 nm (0.1 mJ/pulse) by the frequency-doubled (Inrad Autotracker III) narrow band emission from a dye laser (Lambda Physik FL3002), which was pumped at 308 nm using a XeCl excimer laser (Lextra 100) operating at 2 Hz.

The two laser beams counter-propagated collinearly through the LIF cell. The photolysis laser beam diameter was adjusted to be three times that of the probe laser beam. Red-shifted emission from the radicals was collimated by two convex lenses (f = 10 cm), passed through a long-pass filter (>345 nm), and entered the photomultiplier tube (PMT, R212UH, Hamamatsu Photonics) mounted on top of the cell window orthogonal to the laser beams. The signal from the PMT was amplified (Ortec 9305) before being transmitted to a boxcar averager (SR250, Stanford Research Systems, Inc.) and then sent to the computer data acquisition system (SR245 and SR272). Simultaneously, the LIF signal was transmitted to an oscilloscope for real-time monitoring.

The time delay between the two laser pulses was controlled by a Digital Delay Generator (DG 535). To avoid the scattered light signal from the probe laser, the gate of the boxcar averager was opened 50 ns after the initial rise of the fluorescence signal. The gate width was 25 ns. Scattered light from the interaction of the probe beam with a prism was detected by photodiode 2. The resulting signal was transmitted to boxcar 2 to enable the normalization of the LIF signal to the energy of the probe laser.

The LIF cell consisted of a jacketed 1.3 L Pyrex tube with an inner diameter of 57 mm. Two glass side arms with inner diameters of 19.7 mm were installed at each side of the cell. Quartz windows were attached at Brewster's angle to the end of each arm. To minimize scattered light inside the cell, two conical apertures were installed in the left arm. Both arms were painted black with Krylon black, and the Wood's horn on the bottom was coated with black Aquadag. The temperature in the LIF-cell was controlled between 250 and 335 K by flowing cooled ethanol or heated ethylene glycol through the jacket and was measured with a calibrated thermocouple thermometer (Digi-Sense Dual Input J-T-E-K). The temperatures in the LIF region inside the reaction cell were measured for each pressure with a thermocouple prior to a LIF experiment to ensure accurate temperature measurement. During the LIF experiment, the thermocouple was removed from the LIF region to avoid it scattering the probe laser. The temperature of the cooling and heating liquid was regulated by a temperature bath (Neslab ULT-80).

The fluorescence excitation spectra of $CH_3O\cdot$ and $CD_3O\cdot$ in the range of 285.7−302.7 nm at 296 K show clear progressions in the C−O stretching mode (ν_3), which agrees well with the work of Inoue et al.[54] We chose the peaks at 293.06 and 293.35 nm for monitoring $CH_3O\cdot$ and $CD_3O\cdot$, respectively. In both isotopologues, these are the ($\tilde{A}\ ^2A_1$, $\nu'_3 = 4$) ← ($\tilde{X}^2E$, $\nu''_3 = 0$) transitions, where ν_3 is the C−O stretching mode.[55] All of the LIF signals were corrected for their corresponding background signals, which were obtained by blocking the photolysis beam while only passing the probe beam. The disappearance of methoxy radicals was detected through the change of fluorescence intensity as a function of delay time between the photolysis and probe beams. The shortest delay time used was 5 μs, with the maximum ranging from 30 to 125 μs depending on the concentration of NO_2. For each delay time, 100 to 120 laser shots were taken and averaged.

The initial methoxy radical concentration can be estimated from the absorption cross section of methylnitrite at 351 nm (∼3×10^{-19} cm^2 molecule^{-1}),[32] the quantum yield for the formation of $CH_3O\cdot$ (∼1) at 351 nm,[23,24] the photolysis laser fluence (∼17 mJ pulse^{-1} cm^{-2}), and the methylnitrite concentration (∼3×10^{15} molecules cm^{-3}). The resulting initial concentration of $CH_3O\cdot$ and $CD_3O\cdot$ is ∼2×10^{13} molecules cm^{-3} at 295 K. To establish pseudo-first-order conditions and to avoid side reactions, we used a large excess of NO_2 ($0.9-6 \times 10^{15}$ molecules cm^{-3}) for the kinetic experiments. The temperature range was 250−335 K, and the

dx.doi.org/10.1021/jp501205d | J. Phys. Chem. A 2014, 118, 3552−3563

total pressure was 700 Torr. The gas flow rate was 3360 sccm, and its residence time was 20 s at 295 K and 700 Torr.

III. RESULTS AND DISCUSSION

III-1. Rate Constant Ratio k_{O2}/k_{NO2}. *III-1-1. Results and Preliminary Data Analysis.* Concentrations of CH_3ONO, HCHO, CH_3ONO_2, and CO were obtained from the analysis of the IR spectra. The reproducibility of quantifying ([HCHO] + [CO])/[CH_3ONO_2] varied with the experimental conditions, but typically possessed no more than 5% uncertainty (1 σ). The precision of the determinations of [NO_2] was typically 3%. During the course of reaction, the concentration of CH_3ONO gradually decreased, while the concentrations of the products (HCHO, CH_3ONO_2, and CO) gradually increased. Concentration versus time data from all of the experiments are collected in the Supporting Information (Tables S1−S10).

For each experiment, the concentrations of the products (HCHO, CH_3ONO_2) are plotted against the concentrations of the reactant consumed, and the slope of the linear fit is the yield of the corresponding product. Figure 2 shows plots of product

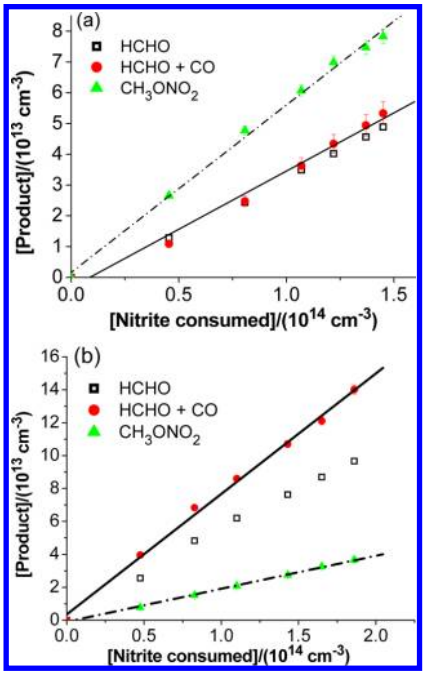

Figure 2. Plot of the product concentration against the reactant consumption at 295 K for the relative rate measurement of CH_3O + O_2/NO_2. (a) A typical plot for the low [O_2]/[NO_2] situation, the concentration ratio between O_2 and NO_2 is 4.60 × 10^3. (b) A typical plot for the high [O_2]/[NO_2] situation, the concentration ratio between O_2 and NO_2 is 4.39 × 10^4. Linear fits are shown for [CH_3ONO_2] and [HCHO] + [CO], but not for [HCHO].

concentration versus the loss of CH_3ONO at low and high [O_2]/[NO_2] ratios at 295 K. The plot for product HCHO shows some nonlinear character largely because secondary chemistry (reactions R5−R7) converted some of the HCHO produced by reaction R1 into CO. Also, HCHO undergoes photolysis via two channels (R8) and (R9) leading to formation of CO; therefore, the formaldehyde formed from R1 can largely be accounted for by adding the observed concentration of CO to the measured HCHO concentration. This is reported below as [HCHO] + [CO].

$$HO_2\cdot + NO \rightarrow NO_2 + \cdot OH \quad (R5)$$

$$HCHO + \cdot OH \rightarrow \cdot CHO + H_2O \quad (R6)$$

$$\cdot CHO + O_2 \rightarrow CO + HO_2\cdot \quad (R7)$$

$$HCHO + h\nu \rightarrow CO + H_2 \quad (R8)$$

$$HCHO + h\nu(+2O_2) \rightarrow CO + 2HO_2\cdot \quad (R9)$$

For the low [O_2]/[NO_2] ratio, the formation of CO from the secondary reaction of formaldehyde is minor, while for the high [O_2]/[NO_2] scenario, the formation of CO due to the OH oxidation of formaldehyde is significant. Similar behavior is observed in the CD_3ONO + O_2/NO_2 experiments, but secondary reactions are less significant upon deuterium substitution. For all experiments, the sum of the product yields is in the range of 80−110% (in terms of moles of carbon) of the methylnitrite lost, which means the spectral analysis captured the major organic products (methylnitrite, formaldehyde, methylnitrate, and CO).

To obtain the pseudo-first-order rate constant ratio between methoxy radical reacting with O_2 and with NO_2, the concentration of formaldehyde (corrected for CO) was plotted against the concentration of methylnitrate, as shown in Figure 3

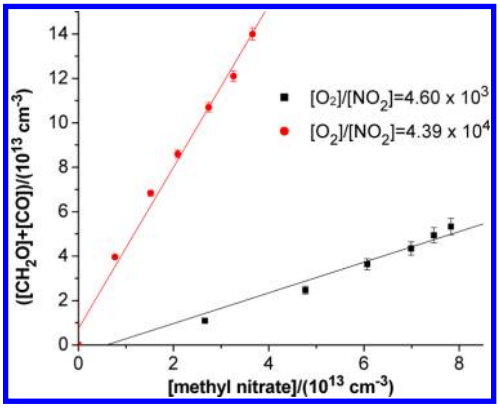

Figure 3. Plot of corrected formaldehyde concentrations ([HCHO] + [CO]) against the concentrations of methylnitrate at 295 K for the relative rate measurement of CH_3O + O_2/NO_2 at a low and high [O_2]/[NO_2]. Error bars shown for [HCHO] + [CO] are 1 σ of the precision of the measurements.

for two sets of experiments with CH_3ONO. From the set of pseudo-first-order rate constants for the complete set of [O_2]/[NO_2] at a given temperature and isotopologue, we can construct a linear least-squares fit to eq 1. For the CH_3ONO + O_2/NO_2 experiments at 295 K we obtain the fit as

$$\frac{k'(O_2)}{k'(NO_2)} = (0.168 \pm 0.030) + (8.394 \pm 0.201) \times 10^{-5} \times \frac{[O_2]}{[NO_2]} \quad (2)$$

where error bars are 1 σ of the precision of the fit. Ratios of pseudo-first-order rate constants for each initial [O_2]/[NO_2] and temperature are listed in Table S11 and Table S12 in the Supporting Information. Pseudo-first-order rate constants from these analyses are provided later, alongside the results reanalyzed as discussed below.

III-1-2. Discussion and Data Reanalysis. The preliminary data analysis above is based on three assumptions: (1) the

dx.doi.org/10.1021/jp501205d | J. Phys. Chem. A 2014, 118, 3552−3563

concentrations of O_2 and NO_2 are constant throughout the experiment; (2) the concentration of HCHO (DCDO) produced from R1 (R3) is equal to the measured HCHO (DCDO) concentration plus the measured CO concentration; and (3) the concentration of CH_3ONO_2 (CD_3ONO_2) produced from R2 (R4) is equal to the measured CH_3ONO_2 (CD_3ONO_2) concentration.

The concentration of O_2 can be treated as constant because the loss of O_2 is negligible compared to the large amount of O_2 present; however, the concentration of NO_2 was not constant. The concentration of NO_2 decreased during the course of reaction by as much as 50%, as is shown in Figure S1 of the Supporting Information. Therefore, the actual concentration of methylnitrate was smaller than what would have been produced if the NO_2 concentration was constant. Figure S1 of the Supporting Information also shows that the NO_2 loss is more severe at low $[O_2]/[NO_2]$, as more of the CH_3O reacts with NO_2 under these conditions. This decrease in $[NO_2]$ is the reason for the curvature and nonzero intercept in Figures 2 and 3.

Corrections were applied to the measured concentrations of methylnitrate to compute the concentration that would have been observed if $[NO_2]$ had been constant. This corrected $[CH_3ONO_2]$ is labeled $[CH_3ONO_2]'$. For the most part, and especially in cases of large NO_2 loss, the time-dependent concentration ratio $[NO_2]_t/[NO_2]_0$ could be well-fit by the empirical three-parameter function (eq 3):

$$\frac{[NO_2]_t}{[NO_2]_0} = y_0 + A\exp\left(-\frac{t}{t_1}\right) \quad (3)$$

For the $CD_3O\cdot$ and most $CH_3O\cdot$ experiments, eq 1 fit the observed $[NO_2]$ to within 5% at all times. The value of $[NO_2]$ extracted from eq 1 was then used to calculate $[CH_3ONO_2]'$. We identify this as correction N1 (Corr_N1), and provide full details in the Supporting Information. Figure 4 shows plots of

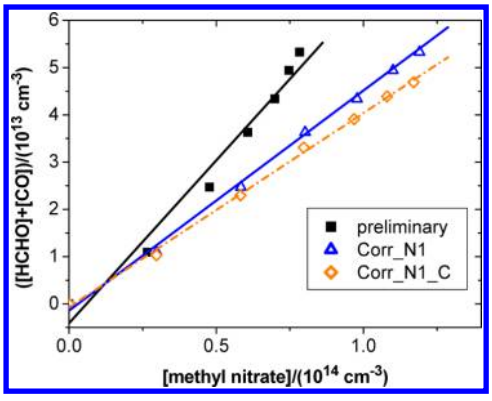

Figure 4. Plot of the original and corrected data at 295 K for one relative rate measurement of $CH_3O + O_2/NO_2$ at $[O_2]/[NO_2]$ of 4.60 × 10^3. Corr_N1 indicates that $[CH_3ONO_2]$ has been corrected for the changing $[NO_2]$, while Corr-N1_C also includes the correction of [HCHO] + [CO] using the predicted results from the model.

[HCHO] + [CO] versus $[CH_3ONO_2]'$ using the same experimental data as in Figure 3 at low $[O_2]/[NO_2]$. Note that Figure 4 also contains results from an additional correction, to be described below. The results from the uncorrected data in the preliminary analysis clearly display curvature, while the corrected results (Corr_N1) display better linearity. A linear least-squares fit of the uncorrected data leads to the following equation:

$$[CH_2O] + [CO] = (-4.1 \pm 2.9) \times 10^{12} + (0.689 \pm 0.050)[CH_3ONO_2] \quad (R^2 = 0.974) \quad (4)$$

The large negative intercept is another consequence of the curvature of the data. After the correction of the CH_3ONO_2 concentration data the linear fit equation becomes

$$[CH_2O] + [CO] = (-1.3 \pm 0.8) \times 10^{12} + (0.458 \pm 0.010)[CH_3ONO_2]' \quad (R^2 = 0.998) \quad (5)$$

For both eq 4 and eq 5, the error bars listed are 1 σ of the precision of the fit. The correction results in a smaller (less negative) intercept and a smaller slope. Although the change in slope is large for this particular case, the change is much smaller in experiments carried out at larger $[O_2]/[NO_2]$ which have a greater influence on the determination of the rate constant ratios (k_1/k_2 or k_3/k_4).

To investigate the validity of the assumption that secondary chemistry does not influence the concentrations of formaldehyde + CO and methylnitrate, the chemistry in the chamber experiments was simulated using Kintecus v.4.35.[56,57] Ideally, we would have used kinetic modeling to fit k_1 and k_3, or to correct the observed methylnitrate concentrations for the loss of NO_2 over the course of the experiments. While our model (see Table S13 of the Supporting Information) captures general trends in the extent of NO_2 loss in the experiments, as shown in Figure S1 of the Supporting Information, it does not quantitatively reproduce the time history of $[NO_2]$.

Kintecus was used with a modified Bader−Deuflhard integrator.[56] Separate models were constructed for each isotopologue. Each model contains 47 reactions and their corresponding temperature-dependent rate constants. The photolysis rate constant for NO_2 (3.3×10^{-4} s^{-1}) was determined from separate experiments, accounting for the secondary chemistry of NO_x and O_x. The photolysis rate constant for methylnitrite (1.5×10^{-4} s^{-1}) was determined by fitting its observed rate of loss at 295 K. The loss of methylnitrite due to its reaction with OH was simulated to be, at most, 2.5% of the total loss; therefore, this assumption introduces minimal error. Typical concentrations of OH radical were 10^6−10^7 cm^{-3} depending on initial conditions and the elapsed photolysis time. NO_2 photolysis and the reaction NO + O_3 caused extensive NO_2 production and loss, although there was also significant loss of NO_x to the formation of $HONO_2$ and CH_3ONO_2. At the highest $[O_2]/[NO_2]$, modeled $[NO_2]$ typically agreed very well with experimental measurements. Unfortunately, the ratio of measured/modeled $[NO_2]$ loss reached a factor of 1.3−1.4 at low $[O_2]/[NO_2]$ toward the middle or end of the photolysis time.

The reaction of OH with CO consumed negligible amounts of CO (<0.3%), and the loss of methylnitrate to photolysis and reaction with OH was similarly low. Although large amounts of HCHO were consumed via R6−R9 (reaction with OH and photolysis to make CO), the effects of these reactions were already taken into account in the data analysis by adding the measured [CO] to the measured [HCHO]. Three additional reactions are potentially significant sources or sinks of HCHO:

dx.doi.org/10.1021/jp501205d | J. Phys. Chem. A 2014, 118, 3552−3563

$$CH_3O\cdot + NO \rightarrow HCHO + HNO \quad (R10)$$

$$\cdot OH + CH_3ONO \rightarrow HCHO + NO + H_2O \quad (R11)$$

$$HO_2\cdot + HCHO \leftrightarrows HOCH_2O_2 \quad (R12)$$

The overall influence of R10−R12 on the modeled [HCHO] + [CO] (%) was computed as $([HCHO] + [CO] - [HCHO]_{R1})/[HCHO]_{R1}) \times 100$, where $[HCHO]_{R1}$ is the [HCHO] produced from R1, alone. Figure 5 illustrates the net

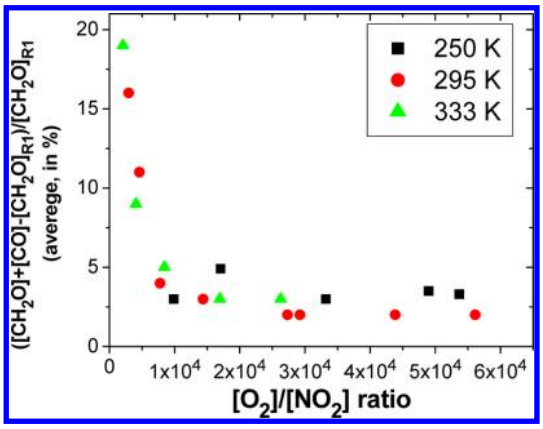

Figure 5. Model results for time-averaged overall influence of R10−R12 to the concentration of HCHO produced by R1 only against the $[O_2]/[NO_2]$ ratio in all experimental conditions for $CH_3ONO + O_2/NO_2$ experiments at 250 K, 295 K, and 333 K.

effect of these reactions on the HCHO + CO concentrations produced by R1. Their effects are only significant at rather low $[O_2]/[NO_2]$, where the sum of the HCHO and CO concentrations is significantly larger than the HCHO produced by R1 due to the HCHO produced via R10 ($CH_3O\cdot$ + NO). This also explains the nonlinearity and negative intercept of the HCHO + CO yield at the low $[O_2]/[NO_2]$ ratio in Figure 2.

Models of results such as those in Figure 5 can be used to correct observed HCHO concentrations and obtain revised ratios of the pseudo-first-order rate constants. A plot of the corrected [HCHO] + [CO] against $[CH_3ONO_2]'$ was included in Figure 4. The new linear fit of [HCHO] + [CO] versus $[CH_3ONO_2]'$ at 295 K at low $[O_2]/[NO_2]$, using the same data used to obtain the fits presented in eq 4 and eq 5, yields

$$[HCHO] + [CO] = (-6.8 \pm 6.3) \times 10^{11} + (0.411 \pm 0.008)[CH_3ONO_2]' \quad (R^2 = 0.998) \quad (6)$$

where the error bars listed are 1 σ of the precision of the fit. Compared to eq 4 and eq 5, this linear fit has a smaller intercept as well as a smaller slope. Note that eqs 4−6 illustrate the effect of these corrections on the data at low $[O_2]/[NO_2]$. The influence of the correction is smaller and even negligible at the higher $[O_2]/[NO_2]$ ratios that largely determine the rate constant ratio. For this reason, and because the correction to $[CH_3ONO_2]$ is smaller at higher $[O_2]/[NO_2]$ ratios, it is highly recommended to use high $[O_2]/[NO_2]$ concentrations in future relative rate constant studies of the methoxy radical reacting with O_2 and NO_2.

Whereas above we applied corrections Corr_N1 and Corr_N1_C to trends in ([HCHO] + [CO]) versus $[CH_3ONO_2]$ at a single $[O_2]/[NO_2]$, we now apply these corrections over a range of $[O_2]/[NO_2]$ concentrations to determine the pseudo-first-order rate constant ratio used in eq 1. Examples for the $CH_3ONO + O_2/NO_2$ experiments at 295 K are shown in eq 7 and eq 8. Figure 6 displays the original

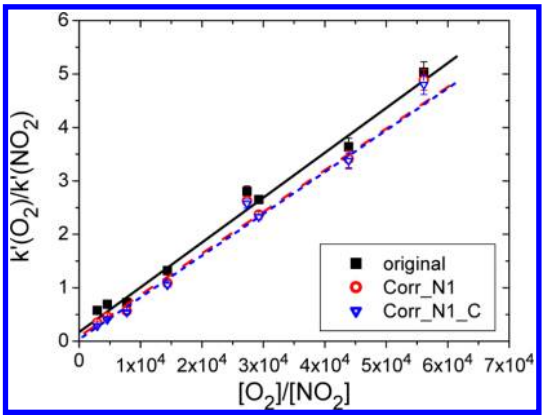

Figure 6. Plot of the pseudo-first-order rate constants against the concentration ratios between O_2 and NO_2 at 295 K for the relative rate measurement of $CH_3O + O_2/NO_2$. The slope of this plot represents the rate constant ratio between O_2 and NO_2 at 295 K, that is, k_1/k_2 (295 K). Correction methods (Corr_N1 and Corr_N1_C) are defined in section III-1-2 of the text.

concentration data on which eq 7 and eq 8 are based and both sets of corrected concentrations as well as fits to all three sets of data.

$$\frac{k'(O_2)}{k'(NO_2)} = (0.087 \pm 0.011) + (7.782 \pm 0.142) \times 10^{-5} \times \frac{[O_2]}{[NO_2]} \quad (7)$$

$$\frac{k'(O_2)}{k'(NO_2)} = (0.036 \pm 0.009) + (7.825 \pm 0.134) \times 10^{-5} \times \frac{[O_2]}{[NO_2]} \quad (8)$$

Eq 7 is the result of a linear fit using the corrected CH_3ONO_2 concentration (Corr_N1). Eq 8 is the result of a linear fit using the corrected CH_3ONO_2 concentration and modeling the correct [HCHO] (Corr_N1_C). The error bars listed are 1 σ of the precision of the fit. Compared to eq 2 (results without correction), using Corr_N1 decreases the positive intercept by 40−50%. The slope of the plot, which represents the ratio of the rate constants between O_2 and NO_2, decreases as well; however, at higher temperatures in the $CH_3ONO + O_2/NO_2$ experiments, the slopes of the plots increase after the correction. When using Corr_N1_C the intercept of the line decreases because the correction factor for HCHO is larger at the lower $[O_2]/[NO_2]$ ratio. However, the change of the slope and, hence, the rate constant ratio, is small and within the error bar.

Similar modeling was carried out for the $CD_3ONO + O_2/NO_2$ reaction system to determine the effect of side reactions on the computed rate constant values. The model of $CD_3ONO + O_2/NO_2$ has larger uncertainties than that of $CH_3ONO + O_2/NO_2$ due to the lack of reports of temperature-dependent rate constants. Table 1 lists rate constant ratios for reactions of CH_3O with O_2 and NO_2, determined using the preliminary analysis of the observed concentration data ("preliminary") and

dx.doi.org/10.1021/jp501205d | J. Phys. Chem. A 2014, 118, 3552−3563

Table 1. Ratios of the Rate Constants for the $CH_3ONO + O_2/NO_2$ (i.e., k_1/k_2) and $CD_3ONO + O_2/NO_2$ (i.e., k_3/k_4) Experiments at All Measured Temperatures[a]

T (K)	preliminary	Corr_N1	Corr_N1_C
		(k_1/k_2) ($\times 10^5$)	
250	5.54 ± 0.28	4.40 ± 0.18	4.32 ± 0.18
265	6.33 ± 0.15	5.26 ± 0.09	5.26 ± 0.09
278	7.08 ± 0.24	7.01 ± 0.15	7.08 ± 0.15
295	8.39 ± 0.20	7.78 ± 0.14	7.83 ± 0.13
316	10.08 ± 0.25	10.51 ± 0.16	10.49 ± 0.16
333	11.44 ± 0.38	12.12 ± 0.17	12.14 ± 0.21
		(k_3/k_4) ($\times 10^5$)	
277	1.61 ± 0.06	1.28 ± 0.04	1.26 ± 0.05
294	1.92 ± 0.04	1.75 ± 0.09	1.70 ± 0.08
319	2.53 ± 0.06	2.33 ± 0.06	2.32 ± 0.06
335	3.17 ± 0.11	2.85 ± 0.10	2.92 ± 0.10

[a]The error bars for all numbers are 1 σ precision of the fit to the product yield ratios. Correction methods (Corr_N1 and Corr_N1_C) are defined in section III-1-2 of the text.

the two different correction methods discussed above. The fully corrected Corr_N1_C results are considered to be most accurate, and represent our best estimate of k_1/k_2 and k_3/k_4. For both $CH_3O\cdot$ and $CD_3O\cdot$, the rate constant ratios determined using Corr_N1_C are no more than 22% lower than the results of the preliminary analyses, with the largest errors at the lowest temperatures. Differences at the higher temperatures are typically 6−8% and the modest extent of these errors is encouraging.

III-2. Absolute Rate Constants for $CH_3O\cdot + NO_2$ and $CD_3O\cdot + NO_2$. We determined the absolute rate constant for $CH_3O\cdot/CD_3O\cdot + NO_2$ (R2/R4) at 700 Torr and temperatures equal to or close to those used in the chamber experiments. Figure 7 shows a typical plot of the logarithm of LIF intensity versus delay time between the photolysis laser pulse and the probe laser pulse for several NO_2 concentrations at 295 K. Pseudo-first-order reaction rate constants, k', were obtained from the slopes of the linear-least-squares fits at each NO_2 concentration. The slope of the plots of k' against NO_2 concentration, determined by linear least-squares fitting, provided the bimolecular reaction rate constants k_2 and k_4 at each temperature and pressure. Figure 8 shows a plot of the pseudo-first-order rate constant versus $[NO_2]$ for multiple temperatures. The high linearity of the data shown in Figures 7 and 8 and the modest intercepts of Figure 8 confirm the applicability of the pseudo-first-order approximation to our experiment and that complications from secondary chemistry are minimal.

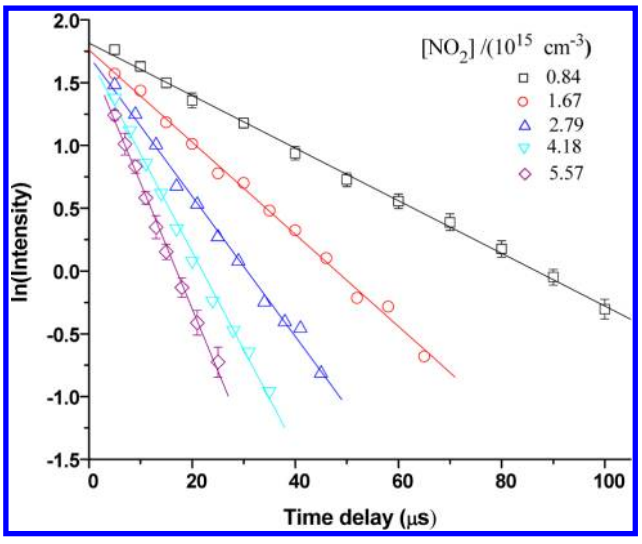

Figure 7. Typical linear decay of ln(LIF intensity) as a function of the delay time for $CH_3O\cdot + NO_2$ at 295 K and a total pressure of 700 Torr. NO_2 concentrations in molecules cm^{-3} are listed in the legend. Error bars (1 σ) are shown at two $[NO_2]$.

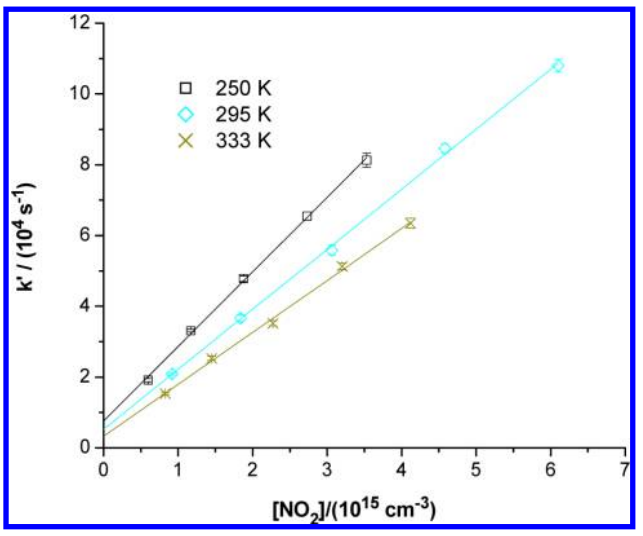

Figure 8. Plot of k'_2 versus $[NO_2]$ at 700 Torr and three temperatures. Error bars are 1 σ precision of the fitted slope of ln(intensity) versus time.

The nonzero y-intercepts in Figure 8 can be interpreted as the sum of the loss rates of $CH_3O\cdot$ for all loss processes other than reaction with NO_2. These processes include (1) diffusion and (2) the reaction primarily with CH_3ONO ($k_{298} = 4.4 \times 10^{-13}$ cm^3 s^{-1}),[58] NO ($k_{298} = 3.6 \times 10^{-11}$ cm^3 s^{-1}),[45] $CH_3O\cdot$ ($k_{298} = 1-4 \times 10^{-11}$ cm^3 s^{-1}),[59−61] and CH_3ONO_2 ($k_{298} = 2.8 \times 10^{-14}$ cm^3 s^{-1}).[45]

Rate constants k_2 and k_4 for methoxy + NO_2 were measured (at 700 Torr) at each temperature that was used in the relative rate measurements at the NCAR. Results are listed in Table 2. A more complete survey of the joint pressure and temperature dependence of k_2 and k_4 will be presented in a subsequent paper.[62] Rate constants k_2 and k_4 are the overall values directly measured by the LFP-LIF method. The rate constant, k_{2b}, for the disproportionation reaction[28] is thought to be less than 2%

Table 2. Rate Constants and KIE for Methoxy + NO_2 at 700 Torr[a]

$CH_3O\cdot + NO_2$		$CD_3O\cdot + NO_2$		
T (K)	k_2 (cm^3 s^{-1} $\times 10^{-11}$)	T (K)	k_4 (cm^3 s^{-1} $\times 10^{-11}$)	KIE (k_2/k_4)
250	2.16 ± 0.04	250	2.18 ± 0.07	0.99 ± 0.04
265	2.01 ± 0.06			
278	1.89 ± 0.03	277	1.93 ± 0.03	0.98 ± 0.04
295	1.70 ± 0.03	294	1.75 ± 0.04	0.97 ± 0.03
316	1.62 ± 0.02	319	1.65 ± 0.03	0.98 ± 0.02
333	1.47 ± 0.03	335	1.53 ± 0.03	0.96 ± 0.03

[a]Cited errors are statistical 1 σ of the precision, and the 5% uncertainty for $[NO_2]$ measurement is not included.

dx.doi.org/10.1021/jp501205d | J. Phys. Chem. A 2014, 118, 3552−3563

of the value of k_2 measured in these experiments. There have not been any studies of the disproportionation reaction for CD_3O + NO_2; however, it is reasonable to assume that deuterium substitution will lower the disproportionation rate constant. In the analysis that follows, we assume that the rate constant observed for the methoxy + NO_2 reaction is equal to the rate of the association reaction to form methylnitrate.

Figure 9 shows the measured values of both k_2 and k_4 as a function of temperature at 700 Torr. By plotting $\ln(k)$ against

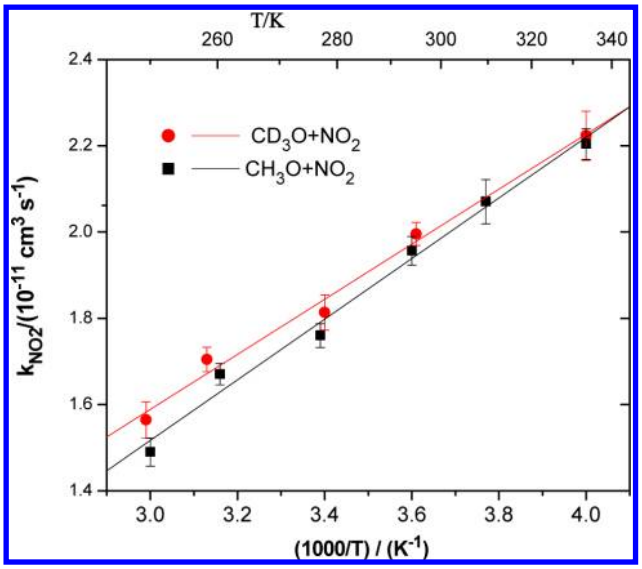

Figure 9. Temperature dependence of methoxy + NO_2 at 700 Torr. Error bars are 1 σ of the precision of the fits to the data.

$1/T$, Arrhenius expressions for the temperature dependence of the rate constants for CH_3O and CD_3O are obtained from the linear least-squares fitting as

$$k_2 = 4.86^{+0.40}_{-0.37} \times 10^{-12} \exp[(374 \pm 24)/T] \text{ cm}^3 \text{ s}^{-1} \quad (9)$$

$$k_4 = 5.59^{+0.59}_{-0.53} \times 10^{-12} \exp[(348 \pm 29)/T] \text{ cm}^3 \text{ s}^{-1} \quad (10)$$

Error bars in eq 9 and eq 10 are 1 σ of the precision of the fits. Both plots show slightly negative temperature dependencies of the rate constants. Values of k_2 are consistently slightly lower than those of k_4, but this difference is not statistically significant. A higher value of k_4 could be rationalized since CD_3ONO_2 has a larger density of states than the normal isotopologue, making the decomposition of CD_3ONO_2 back to reactants slower.[63]

III-3. Rate Constant for CH_3O· + O_2 and CD_3O· + O_2 and Tunneling Effect. By combining the rate constant ratios k_1/k_2 and k_3/k_4 determined in part A with the absolute rate constants k_2 and k_4 determined in part B, we can calculate the absolute rate constants k_1 and k_3 at 700 Torr over the whole temperature range of our experiment. The results of these calculations are shown in Table 3. The temperature dependence of k_1 and k_3 at 700 Torr is plotted in Figure 10. The

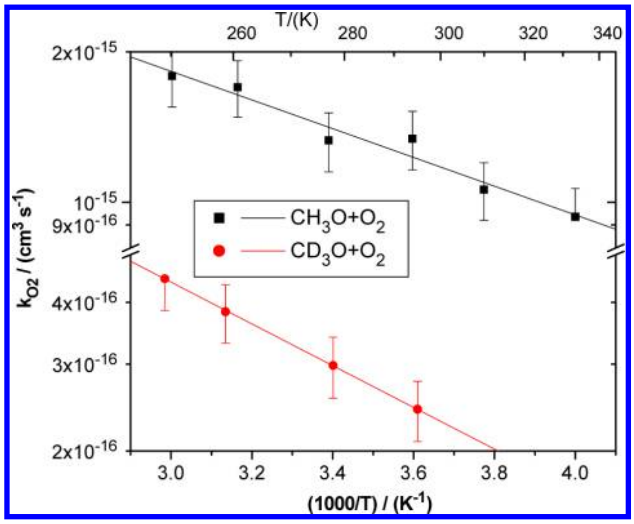

Figure 10. Temperature dependence of methoxy + O_2 at 700 Torr. The solid lines represent the linear least-squares fit to the data.

uncertainty in k_1 and k_3 arise from uncertainties in both the relative rate study and the measurement of methoxy + NO_2. The following Arrhenius expressions are derived for k_1 and k_3 from the present work:

$$k_1 = 1.3^{+0.9}_{-0.5} \times 10^{-14} \exp[-(663 \pm 144)/T] \text{ cm}^3 \text{ s}^{-1} \quad (11)$$

$$k_3 = 8.2^{+7.7}_{-4.0} \times 10^{-15} \exp[-(974 \pm 210)/T] \text{ cm}^3 \text{ s}^{-1} \quad (12)$$

The uncertainties above are 1 σ and include uncertainty in the absorption cross-section for methylnitrate (10%), formaldehyde, CO, and NO_2.

Both k_1 and k_3 show positive temperature dependencies. Note that the reaction methoxy + O_2 is bimolecular,[36−38] and therefore, the rate constant is expected to be independent of the pressure. Consequently, it is valid to compare our results with previous absolute rate measurements carried out at lower pressures (<100 Torr).[3−5,19] Compared to the Arrhenius fitting of previous experimental data on R1 over 298−610 K by Orlando et al.,[19] the pre-exponential factor for k_1 in this study ($1.3^{+0.9}_{-0.5} \times 10^{-14}$ cm^3 s^{-1}) is a factor of 6 smaller, and the activation energy (1.3 ± 0.3 kcal/mol) is approximately 40% smaller. We combined our results together with previous experimental data for k_1 in Figure 11 over the temperature

Table 3. Absolute Rate Constant for k_1 and k_3 (unit: cm^3 s^{-1}) and the KIE[a]

T (K)	250	265	278	295	316	333
k_1 (× 10^{15})	0.94 ± 0.13	1.06 ± 0.14	1.34 ± 0.18	1.33 ± 0.18	1.70 ± 0.22	1.79 ± 0.24
T (K)			277	294	319	335
k_3 (× 10^{16})			2.43 ± 0.34	2.98 ± 0.42	3.83 ± 0.52	4.46 ± 0.62
KIE (this work)			5.50 ± 0.28	4.46 ± 0.26	4.44 ± 0.16	4.00 ± 0.19
KIE (ref 38)	4.6	4.2	4.0	3.7	3.5	3.3

[a]The quoted errors (1 σ) include statistical uncertainties from the linear fitting of both the relative and absolute rate methods. The error bars for the rate constants, but not the KIE, include the uncertainties in the literature value of the absorption cross-sections of methylnitrate, formaldehyde, and CO in the NCAR experiments, and the absorption cross-section of NO_2 in both experiments.

dx.doi.org/10.1021/jp501205d | J. Phys. Chem. A 2014, 118, 3552−3563

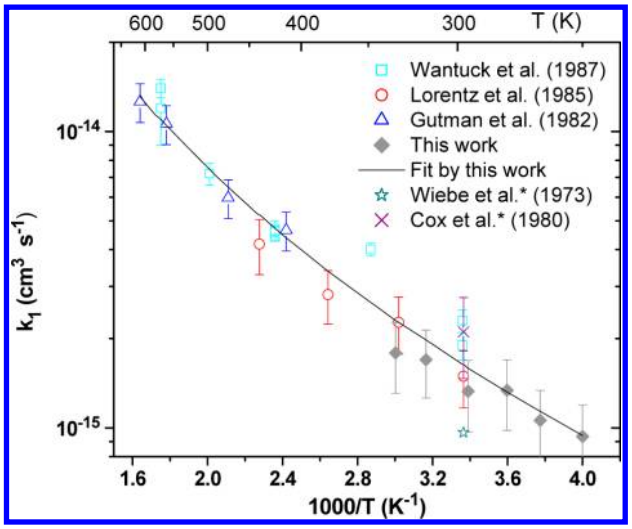

Figure 11. Temperature-dependent rate constant for $CH_3O + O_2$ in the range of 250−610 K. The solid line represents the modified Arrhenius fit of eq 13. Among the previous experimental data, the ones from Wiebe et al. and Cox et al. at 298 K (denoted by*) were derived by combining the originally determined relative rate constant with the absolute rate constant for the reference reaction measured in the current work (R2) or elsewhere ($CH_3O· + NO$).[45] Error bars on our work are 2 σ error bars on combined precision and accuracy.

range 250−610 K. There is reasonable agreement between our results and the absolute results from Lorentz et al. in the overlapping temperature range (298−333 K); however, our data (below room temperature) exhibit less temperature dependence for k_1, which is the source of our lower activation energy and pre-exponential factor.

The data in Figure 11 appear to exhibit some curvature and can be fit by a modified Arrhenius form as

$$k_1 = 3.8 \times 10^{-21}\, T^{2.40} \exp(-208/T)\ \text{cm}^3\ \text{s}^{-1} \quad (13)$$

We include this parametrization in Figure 11.

KIEs are reported in Table 3 for each temperature for which k_1 and k_3 were obtained. The KIE values obtained here (4.0−5.5) are far smaller than the value of ∼100 determined in one previous study.[34] Note that the theoretical study of ref 38, also listed in Table 3, yielded slightly smaller KIEs and a more modest temperature dependence of the KIEs than was observed in the present experiments. Another way to express the KIE is in the Arrhenius form (with 1 σ error bars on precision, to the fits of k_1/k_2, k_3/k_4, k_2, and k_4):

$$k_1/k_3 = (1.7^{+0.5}_{-0.4}) \exp\left(\frac{306 \pm 70}{T}\right) \quad (14)$$

Several studies proposed that an A_H/A_D of <1.0[64−66] or <0.5[67] signal that tunneling is important. Similarly, the difference in activation energy $E_D - E_H$ > 1.2−1.4 kcal/mol[64−66] is also proposed as a criterion for tunneling. If both criteria are met, the tunneling coefficient, κ, for the normal hydrogen is typically greater than ∼5.[66] In our results, neither A_H/A_D ($1.6^{+2.1}_{-0.9}$) nor $E_D - E_H$ (0.6 ± 0.5 kcal/mol) suggests that κ is nearly as high as 5. This is qualitatively consistent with the conclusion from our measurements of the branching ratios for the reaction of $CH_2DO· + O_2$.[39] An oddity of the theoretical findings in ref. 38 was that tunneling was computed to be of similar importance for both the $CH_3O· + O_2$ and $CD_3O· + O_2$ reactions. For the normal isotopologue, κ rose from 1.9 to 3.4 as the temperature fell from 330 to 250 K. Over the same range, κ in the deuterated isotopologue rose from 1.8 to 2.5.

Along with previous studies of the methoxy + NO_2 reaction, our work suffers from ignorance of the extent of formation of methyl-peroxy-nitrite (CH_3OONO):

$$CH_3O· + NO_2(+M) \leftrightarrows CH_3OONO \quad (R2c)$$

This weakly bound species[68−70] may dissociate on a time scale slower than that of the LFP-LIF experiments, but certainly dissociates faster than the time scale of the chamber experiments. While there is experimental evidence enabling the quantification of the HOONO formation channel in the HO + NO_2 reaction,[71] there is not even any direct experimental evidence for the occurrence of R2c. Obviously, if formation of CH_3OONO (or CD_3OONO) occurs to a significant extent, the Troe fitting to k_2 and k_4 determined in our LFP-LIF experiment is being applied to the sum of two reactions. In the OH + NO_2 reaction, the branching fraction for the analogue of R2c, formation of peroxy nitrate (HOONO), decreases with increases in temperature (at 700 Torr).[45] If this trend holds for R2, and if methyl-peroxy-nitrite is stable on the time scale of our LFP-LIF experiments, then R2c would contribute more error in our determination of k_1 at the lower temperatures than at the higher temperatures used in our experiments. As our results for k_1 disagree with previous work at the higher temperatures, R2c appears unlikely to be a major factor confounding our results.

IV. CONCLUSION

Our relative rate measurement for $CH_3O· + O_2/NO_2$ and the absolute rate measurement for $CH_3O· + NO_2$ combined together have enabled us to determine the absolute rate constant (k_1) for $CH_3O· + O_2$ in the temperature range of 250−333 K and at 700 Torr. This enabled us to carry out the first determination of k_1 below room temperature. These data are thus of broader relevance to the atmosphere than previously reported values of k_1. Our results show reasonable agreement with previous absolute rate studies in the overlapping temperature range (298−333 K); however, they exhibit less temperature dependence for k_1 than previous data that was obtained at higher temperatures.

By carrying out the same experiments for the isotopologue $CD_3O·$ in the temperature range of 277−335 K, we were able to determine the kinetic isotope effect ($k_H/k_D = k_1/k_3$) for methoxy + O_2. The measured KIEs do not seem greatly affected by tunneling. The KIEs reported here are similar to, if slightly higher than, those computed from theory.[38]

We hope that the experimentally determined $k_1(T)$ for methoxy + O_2 will be helpful to further validate a computational method for this reaction. A validated method would, hopefully, enable reliable and affordable computational studies for RO· + O_2 reactions for larger and functionalized alkoxy radicals derived from atmospherically important compounds such as isoprene or oxygenated VOCs. This would, in turn, enable researchers to extract absolute rate constants for the decomposition and isomerization of these alkoxy radicals from relative rate experiments. These absolute rate constants are necessary to build structure−reactivity relations for unimolecular reactions of the broad array of functionalized alkoxy radicals that are difficult to study experimentally.

dx.doi.org/10.1021/jp501205d | J. Phys. Chem. A 2014, 118, 3552−3563

■ ASSOCIATED CONTENT

Supporting Information

Initial conditions and concentrations of reactants and products versus time for relative rate studies, along with pseudo-first-order rate constant ratios ($k'(O_2)/k'(NO_2)$) for each experiment and expanded discussion of data reanalysis, including the Kintecus model of $CH_3ONO + O_2/NO_2$; experimental conditions and pseudo-first-order rate constants for LFP-LIF studies. This material is available free of charge via the Internet at http://pubs.acs.org.

■ AUTHOR INFORMATION

Corresponding Authors

*E-mail: tsdibble@esf.edu.

*E-mail: tyndall@ucar.edu.

Notes

The authors declare no competing financial interest.

■ ACKNOWLEDGMENTS

J.C., H.H., and T.S.D. gratefully acknowledge support from the National Science Foundation under Grant No. ATG-0937626. The National Center for Atmospheric Research is sponsored by the National Science Foundation. The authors thank David J. Kieber and two anonymous reviewers for their close reading of the manuscript and many helpful suggestions.

■ REFERENCES

(1) Jenkin, M. E.; Clemitshaw, K. C. Ozone and Other Secondary Photochemical Pollutants: Chemical Processes and their Formation in the Planetary Boundary Layer. *Atmos. Environ.* **2000**, *34*, 2499−2527.

(2) Lim, Y. B.; Ziemann, P. J. Products and Mechanism of Secondary Organic Aerosol Formation from Reactions of *n*-Alkanes with OH Radicals in the Presence of NO_x. *Environ. Sci. Technol.* **2005**, *39*, 9229−9236.

(3) Wantuck, P. J.; Oldenborg, R. C.; Baughcum, S. L.; Winn, K. R. Removal Rate Constant Measurements for Methoxy Radical by Oxygen over the 298−973 K Range. *J. Phys. Chem.* **1987**, *91*, 4653−4655.

(4) Gutman, D.; Sanders, N.; Butler, J. Kinetics of the Reactions of Methoxy and Ethoxy Radicals with Oxygen. *J. Phys. Chem.* **1982**, *86*, 66−70.

(5) Lorenz, K.; Rhäsa, D.; Zellner, R.; Fritz, B. Laser Photolysis-LIF Kinetic Studies of the Reactions of CH_3O and CH_2CHO with O_2 between 300 and 500 K. *Ber. Bunsen-Ges. Phys. Chem.* **1985**, *89*, 341−342.

(6) Balla, R. J.; Nelson, H.; McDonald, J. Kinetics of the Reactions of Iso-propoxy Radicals with NO, NO_2, and O_2. *Chem. Phys.* **1985**, *99*, 323−335.

(7) Hartmann, D.; Karthäuser, J.; Sawerysyn, J.; Zellner, R. Kinetics and HO_2 Product Yield of the Reaction $C_2H_5O + O_2$ between 295 and 411 K. *Bunsen-Ges. Phys. Chem., Ber.* **1990**, *94*, 639−645.

(8) Deng, W.; Wang, C.; Katz, D. R.; Gawinski, G. R.; Davis, A. J.; Dibble, T. S. Direct Kinetic Studies of the Reactions of 2-Butoxy Radicals with NO and O_2. *Chem. Phys. Lett.* **2000**, *330*, 541−546.

(9) Deng, W.; Davis, A. J.; Zhang, L.; Katz, D. R.; Dibble, T. S. Direct Kinetic Studies of Reactions of 3-Pentoxy Radicals with NO and O_2. *J. Phys. Chem. A* **2001**, *105*, 8985−8990.

(10) Fittschen, C.; Frenzel, A.; Imrik, K.; Devolder, P. Rate Constants for the Reactions of C_2H_5O, *i*-C_3H_7O, and *n*-C_3H_7O with NO and O_2 as a Function of Temperature. *Int. J. Chem. Kinet.* **1999**, *31*, 860−866.

(11) Mund, C.; Fockenberg, C.; Zellner, R. LIF spectra of *n*-Propoxy and *i*-Propoxy Radicals and Kinetics of their Reactions with O_2 and NO_2. *Bunsen-Ges. Phys. Chem., Ber.* **1998**, *102*, 709−715.

(12) Hein, H.; Hoffmann, A.; Zellner, R. Direct Investigations of Reactions of 1-Butoxy and 1-Pentoxy Radicals Using Laser Pulse Initiated Oxidation: Reactions with O_2 and Isomerisation at 293 K and 50 mbar. *Phys. Chem. Chem. Phys.* **1999**, *1*, 3743−3752.

(13) Hein, H.; Hoffmann, A.; Zellner, R. Direct Investigations of Reactions of 2-Butoxy Radicals Using Laser Pulse Initiated Oxidation: Reaction with O_2 and Unimolecular Decomposition at 293 K and 50 mbar. *Bunsen-Ges. Phys. Chem., Ber.* **1998**, *102*, 1840−1849.

(14) Zhang, L.; Kitney, K. A.; Ferenac, M. A.; Deng, W.; Dibble, T. S. LIF Spectra of Cyclohexoxy Radical and Direct Kinetic Studies of Its Reaction with O_2. *J. Phys. Chem. A* **2004**, *108*, 447−454.

(15) Zhang, L.; Callahan, K. M.; Derbyshire, D.; Dibble, T. S. Laser-Induced Fluorescence Spectra of 4-Methylcyclohexoxy Radical and Perdeuterated Cyclohexoxy Radical and Direct Kinetic Studies of Their Reactions with O_2. *J. Phys. Chem. A* **2005**, *109*, 9232−9240.

(16) Wu, F.; Carr, R. W. Kinetics of CH_2ClO Radical Reactions with O_2 and NO, and the Unimolecular Elimination of HCl. *J. Phys. Chem. A* **2001**, *105*, 1423−1432.

(17) Wu, F.; Carr, R. W. The Chloromethoxy Radical: Kinetics of the Reactions with O_2 and the Unimolecular Elimination of HCl at 306 K. *Chem. Phys. Lett.* **1999**, *305*, 44−50.

(18) Wu, F.; Carr, R. W. Kinetic Study of the Reaction of the $CFCl_2CH_2O$ Radical with O_2. *J. Phys. Chem.* **1996**, *100*, 9352−9359.

(19) Orlando, J. J.; Tyndall, G. S.; Wallington, T. J. The Atmospheric Chemistry of Alkoxy Radicals. *Chem. Rev.* **2003**, *103*, 4657−4690.

(20) Atkinson, R. Rate Constants for the Atmospheric Reactions of Alkoxy Radicals: An Updated Estimation Method. *Atmos. Environ.* **2007**, *41*, 8468−8485.

(21) Barker, J. R.; Benson, S. W.; Golden, D. M. The Decomposition of Dimethyl Peroxide and the Rate Constant for $CH_3O + O_2 \rightarrow CH_2O + HO_2$. *Int. J. Chem. Kinet.* **1977**, *9*, 31−53.

(22) Batt, L.; Robinson, G. Reaction of Methoxy Radicals with Oxygen. I. Using Dimethyl Peroxide as a Thermal Source of Methoxy Radicals. *Int. J. Chem. Kinet.* **1979**, *11*, 1045−1053.

(23) Cox, R.; Derwent, R.; Kearsey, S.; Batt, L.; Patrick, K. Photolysis of Methyl Nitrite: Kinetics of the Reactions of the Methoxy Radical with O_2. *J. Photochem.* **1980**, *13*, 149−163.

(24) Wiebe, H.; Villa, A.; Hellman, T.; Heicklen, J. Photolysis of Methyl Nitrite. *J. Am. Chem. Soc.* **1973**, *95*, 7−13.

(25) Glasson, W. A. Methoxyl Radical Reactions in Atmospheric Chemistry. *Environ. Sci. Technol.* **1975**, *9*, 1048−1053.

(26) Mendenhall, G. D.; Golden, D. M.; Benson, S. W. The Very-Low-Pressure Pyrolysis (VLPP) of *n*-Propyl Nitrate, *tert*-Butyl Nitrite, and Methyl Nitrite. Rate Constants for Some Alkoxy Radical Reactions. *Int. J. Chem. Kinet.* **1975**, *7*, 725−737.

(27) Wantuck, P. J.; Oldenborg, R. C.; Baughcum, S. L.; Winn, K. R. Collisional Quenching of Methoxy (A^2A_1) Radical. *J. Phys. Chem.* **1987**, *91*, 3253−3259.

(28) McCaulley, J.; Anderson, S.; Jeffries, J.; Kaufman, F. Kinetics of the Reaction of CH_3O with NO_2. *Chem. Phys. Lett.* **1985**, *115*, 180−186.

(29) Biggs, P.; Canosa-Mas, C. E.; Fracheboud, J. M.; Parr, A. D.; Shallcross, D. E.; Wayne, R. P.; Caralp, F. Investigation into the Pressure Dependence between 1 and 10 Torr of the Reactions of NO_2 with CH_3 and CH_3O. *J. Chem. Soc., Faraday Trans.* **1993**, *89*, 4163−4169.

(30) Frost, M. J.; Smith, I. W. Rate Constants for the Reactions of CH_3O and C_2H_5O with NO_2 over a Range of Temperature and Total Pressure. *J. Chem. Soc., Faraday Trans.* **1990**, *86*, 1751−1756.

(31) Frost, M. J.; Smith, I. W. Corrigendum to Rate Constants for the Reactions of CH_3O and C_2H_5O with NO_2 over a Range of Temperature and Total Pressure. *J. Chem. Soc., Faraday Trans.* **1993**, *89*, 4251.

(32) Wollenhaupt, M.; Crowley, J. Kinetic Studies of the Reactions $CH_3 + NO_2 \rightarrow$ Products, $CH_3O + NO_2 \rightarrow$ Products, and $OH + CH_3C(O)CH_3 \rightarrow CH_3C(O)OH + CH_3$, over a Range of Temperature and Pressure. *J. Phys. Chem. A* **2000**, *104*, 6429−6438.

(33) Martínez, E.; Albaladejo, J.; Jiménez, E.; Notario, A.; Díaz de Mera, Y. Temperature Dependence of the Limiting Low- and High-pressure Rate Constants for the $CH_3O + NO_2 + He$ Reaction over the

250−390 K Temperature Range. *Chem. Phys. Lett.* **2000**, *329*, 191−199.
(34) Weaver, J.; Shortridge, R.; Meagher, J.; Heicklen, J. The Photooxidation of $CD_3N_2CD_3$. *J. Photochem.* **1975**, *4*, 109−120.
(35) Jungkamp, T. P.; Seinfeld, J. H. The Mechanism of Methoxy Radical Oxidation: Hydrogen Abstraction versus Trioxy Radical Formation. *Chem. Phys. Lett.* **1996**, *263*, 371−378.
(36) Bofill, J. M.; Olivella, S.; Solé, A.; Anglada, J. M. The Mechanism of Methoxy Radical Oxidation by O_2 in the Gas Phase. Computational Evidence for Direct H Atom Transfer Assisted by an Intermolecular Noncovalent O···O Bonding Interaction. *J. Am. Chem. Soc.* **1999**, *121*, 1337−1347.
(37) Setokuchi, O.; Sato, M. Direct Dynamics of an Alkoxy Radical (CH_3O, C_2H_5O, and *i*-C_3H_7O) Reactions with an Oxygen Molecule. *J. Phys. Chem. A* **2002**, *106*, 8124−8132.
(38) Hu, H.; Dibble, T. S. Quantum Chemistry, Reaction Kinetics, and Tunneling Effects in the Reaction of Methoxy Radicals with O_2. *J. Phys. Chem. A* **2013**, *117*, 14230−14242.
(39) Hu, H.; Dibble, T. S.; Tyndall, G. S.; Orlando, J. J. Temperature-Dependent Branching Ratios of Deuterated Methoxy Radicals ($CH_2DO\cdot$) Reacting With O_2. *J. Phys. Chem. A* **2012**, *116*, 6295−6302.
(40) Blatt, A. H. *Organic Syntheses*; Wiley: New York, 1966; pp 108−109.
(41) Taylor, W.; Allston, T.; Moscato, M.; Fazekas, G.; Kozlowski, R.; Takacs, G. Atmospheric Photodissociation Lifetimes for Nitromethane, Methyl Nitrite, and Methyl Nitrate. *Int. J. Chem. Kinet.* **1980**, *12*, 231−240.
(42) Rook, F. L. Preparation, Vapor Pressure, and Infrared Spectrum of Methyl Nitrite. *J. Chem. Eng. Data* **1982**, *27*, 72−73.
(43) Calvert, J. G.; Pitts, J. N. *Photochemistry*; Wiley: New York, 1966; pp 455.
(44) Mabbott, G. A. A Simple Infrared Cell for Gases. *J. Chem. Educ.* **1995**, *72*, 471−472.
(45) Sander, S. P.; Friedl, R. R.; Barker, J. R.; Golden, D. M.; Kurylo, M. J.; Abbatt, J. P. D.; Burkholder, J. B.; Kolb, C. E.; Moortgat, G. K.; Huie, R. E.; et al. *Chemical Kinetics and Photochemical Data for Use in Atmospheric Studies Evaluation, Number 17*; JPL Publication: Pasadena, 2011; pp 10−6.
(46) Shetter, R.; Davidson, J.; Cantrell, C.; Calvert, J. Temperature Variable Long Path Cell for Absorption Measurements. *Rev. Sci. Instrum.* **1987**, *58*, 1427.
(47) Tyndall, G. S.; Orlando, J. J.; Calvert, J. G. Upper Limit for the Rate Coefficient for the Reaction $HO_2 + NO_2 \rightarrow HONO + O_2$. *Environ. Sci. Technol.* **1995**, *28*, 202−206.
(48) Tuazon, E. C.; Atkinson, R. A Product Study of the Gas-Phase Reactions of Isoprene with the OH Radical in the Presence of NO_x. *Int. J. Chem. Kinet.* **1990**, *22*, 1221−1236.
(49) Orlando, J. J.; Iraci, L. T.; Tyndall, G. S. Chemistry of the Cyclopentoxy and Cyclohexoxy Radicals at Subambient Temperatures. *J. Phys. Chem. A* **2000**, *104*, 5072−5079.
(50) Staffelbach, T. A.; Orlando, J. J.; Tyndall, G. S.; Calvert, J. G. The UV-visible Absorption Spectrum and Photolysis Quantum Yields of Methylglyoxal. *J. Geophys. Res.* **1995**, *100*, 14189−14198.
(51) Gratien, A.; Nilsson, E.; Doussin, J.; Johnson, M. S.; Nielsen, C. J.; Stenstrøm, Y.; Picquet- Varrault, B. UV and IR absorption Cross-Sections of HCHO, HCDO, and DCDO. *J. Phys. Chem. A* **2007**, *111*, 11506−11513.
(52) Tyndall, G. S.; Orlando, J.; Nickerson, K. E.; Cantrell, C.; Calvert, J. An Upper Limit for the Rate Coefficient of the Reactions of NH_2 Radicals with O_2 Using FTIR Product Analysis. *J. Geophys. Res.* **1991**, *96*, 20761−20768.
(53) Wang, C.; Shemesh, L. G.; Deng, W.; Lilien, M. D.; Dibble, T. S. Laser-Induced Fluorescence Excitation Spectra of *tert*-Butoxy and 2-Butoxy Radicals. *J. Phys. Chem. A* **1999**, *103*, 8207−8212.
(54) Inoue, G.; Akimoto, H.; Okuda, M. Spectroscopy of the CH_3O A^2A_1-X^2E System by Laser Excited Fluorescence Method. *J. Chem. Phys.* **1980**, *72*, 1769−1775.
(55) Foster, S. C.; Misra, P.; Lin, T. Y. D.; Damo, C. P.; Carter, C. C.; Miller, T. A. Free Jet Cooled Laser-Induced Fluorescence Spectrum of Methoxy. 1. Vibronic Analysis of the Ã and X States. *J. Phys. Chem.* **1988**, *92*, 5914−5921.
(56) Ianni, J. C. A Comparison of the Bader-Deuflhard and the Cash-Karp Runge-Kutta Integrators for the GRI-MECH 3.0 Model Based on the Chemical Kinetics Code Kintecus. In *Computational Fluid and Solid Mechanics*; Bathe, K. J., Ed.; Elsevier Science Ltd.: Oxford, UK, 2003; pp 1368−1372.
(57) Ianni, J. C. *Kintecus, Windows Version 4.35*, 2011. http://kintecus.com/.
(58) Albaladejo, J.; Jiménez, E.; Notario, A.; Cabañas, B.; Martínez, E. CH_3O Yield in the $CH_3 + O_3$ Reaction Using the LP/LIF Technique at Room Temperature. *J. Phys. Chem. A* **2002**, *106*, 2512−2519.
(59) Biggs, P.; Canosa-Mas, C. E.; Fracheboud, J.; Shallcross, D. E.; Wayne, R. P. Kinetics of the Reaction of F Atoms with CH_3ONO and CH_3O, and the Reaction of CH_3O with a Number of Hydrocarbons. *J. Chem. Soc., Faraday Trans.* **1997**, *93*, 2481−2486.
(60) Meier, U.; Grotheer, H.; Riekert, G.; Just, T. Study of Hydroxyl Reactions with Methanol and Ethanol by Laser-Induced Fluorescence. *Bunsen-Ges. Phys. Chem., Ber.* **1985**, *89*, 325−327.
(61) Hassinen, E.; Koskikallio, J. Flash Photolysis of Methyl Acetate in Gas Phase. Products and Rate Constants of Reactions between Methyl, Methoxy, and Acetyl Radicals. *Acta Chem. Scand., Ser. A* **1979**, *33*, 625.
(62) Chai, J.; Dibble, T. S. Pressure Dependence and Kinetic Isotope Effects in the Absolute Rate Constant for Methoxy Radical Reacting with NO_2. *Int. J. Chem. Kinet.*, submitted for publication.
(63) Baer, T.; Hase, W. L. *Unimolecular Reaction Dynamics: Theory and Experiments*; Oxford Univ. Press: New York, 1996; 266−267.
(64) Kim, Y.; Kreevoy, M. M. The Experimental Manifestations of Corner-Cutting Tunneling. *J. Am. Chem. Soc.* **1992**, *114*, 7116−7123.
(65) Caldin, E. F. Tunneling in Proton-transfer Reactions in Solution. *Chem. Rev.* **1969**, *69*, 135−156.
(66) Pu, J.; Gao, J.; Truhlar, D. G. Multidimensional Tunneling, Recrossing, and the Transmission Coefficient for Enzymatic Reactions. *Chem. Rev.* **2006**, *106*, 3140−3169.
(67) Schneider, M. E.; Stern, M. J. Arrhenius Preexponential Factors for Primary Hydrogen Kinetic Isotope Effects. *J. Am. Chem. Soc.* **1972**, *94*, 1517−1522.
(68) Pan, X.; Fu, Z.; Li, Z.; Sun, C.; Sun, H.; Su, Z.; Wang, R. Theoretical Study on the Mechanism of the Gas-phase Radical−Radical Reactions of CH_3O with NO_2. *Chem. Phys. Lett.* **2005**, *409*, 98−104.
(69) Lesar, A.; Hodošček, M.; Drougas, E.; Kosmas, A. M. Quantum Mechanical Investigation of the Atmospheric Reactions CH_3O_2 + NO. *J. Phys. Chem. A* **2006**, *110*, 7898−7903.
(70) Arenas, J. F.; Avila, F. J.; Otero, J. C.; Pelaez, D.; Soto, J. Approach to the Atmospheric Chemistry of Methyl Nitrate and Methylperoxy Nitrite. Chemical Mechanisms of their Formation and Decomposition Reactions in the Gas Phase. *J. Phys. Chem. A* **2008**, *112*, 249−255.
(71) Mollner, A. K.; Valluvadasan, S.; Feng, L.; Sprague, M. K.; Okumura, M.; Milligan, D. B.; Bloss, W. J.; Sander, S. P.; Martien, P. T.; Harley, R. A. Rate of Gas Phase Association of Hydroxyl Radical and Nitrogen Dioxide. *Science* **2010**, *330*, 646−649.